REPORT DOCUMENTATION PAGE

Form Approved
OMB No. 0704-0188

PLEASE DO NOT RETURN YOUR FORM TO THE ABOVE ORGANIZATION.

1. REPORT DATE *(DD-MM-YYYY)*	2. REPORT TYPE	3. DATES COVERED *(From - To)*
04-19-2017	Conference paper	1 Jan 2014 - 1 Mar 2015

4. TITLE AND SUBTITLE
Optimal Guidance Trajectories for a Nanosat Docking with a Non-Cooperative Resident Space Object

5a. CONTRACT NUMBER
N/A

5b. GRANT NUMBER
N/A

5c. PROGRAM ELEMENT NUMBER
N/A

6. AUTHOR(S)
Parv Patel, Bogdan Udrea, Michael Nayak

5d. PROJECT NUMBER
N/A

5e. TASK NUMBER
N/A

5f. WORK UNIT NUMBER
N/A

7. PERFORMING ORGANIZATION NAME(S) AND ADDRESS(ES)
Air Force Institute of Technology, 2950 Hobson Way, Wright Patterson AFB, OH 45433
Embry-Riddle Aeronautical University, 600 S Clyde Morris Blvd, Daytona Beach FL 32114
University of Southern California, 3620 South Vermont Avenue, Los Angeles, CA 90089

8. PERFORMING ORGANIZATION REPORT NUMBER
N/A

9. SPONSORING/MONITORING AGENCY NAME(S) AND ADDRESS(ES)
Air Force Institute of Technology, 2950 Hobson Way, Wright Patterson AFB, OH 45433

10. SPONSOR/MONITOR'S ACRONYM(S)
AFIT/CIP

11. SPONSOR/MONITOR'S REPORT NUMBER(S)
N/A

12. DISTRIBUTION/AVAILABILITY STATEMENT
Distribution A. Approved for public release: distribution unlimited.

13. SUPPLEMENTARY NOTES
2015 IEEE Aerospace Conference, Mar 7-14, 2015, Big Sky, Montana, MT, USA

14. ABSTRACT

There has been an increasing interest in on-orbit autonomous servicing and repair of satellites as well as controlled active debris removal (ADR) in the space industry recently. One of the most challenging tasks for servicing/repair as well as for ADR is the rendezvous and docking with a non-cooperative tumbling resident space object (RSO). This paper presents a propellant optimal maneuver profile for a servicing spacecraft to perform proximity operations and eventually dock with a non-cooperative target. The strategy is to find an optimal trajectory which will guide the servicing spacecraft to approach the tumbling satellite such that the two vehicles will eventually have no relative motion. Therefore, a subsequent docking or capture operation can be safely performed. The research described here elaborates on the previous work that studied the considering a full six-degree-of-freedom model of both chaser and target. The current work expands the scope by adding new set of linearized equations of motion that capture the effect of the J2 geopotential disturbance force.

15. SUBJECT TERMS
Nanosatellite, laser rangefinder, ARAPAIMA, USAF, object imaging, shape reconstruction, space-based, ISR, space situational awareness, active debris removal, small satellite

16. SECURITY CLASSIFICATION OF:			17. LIMITATION OF ABSTRACT	18. NUMBER OF PAGES	19a. NAME OF RESPONSIBLE PERSON
a. REPORT	b. ABSTRACT	c. THIS PAGE			MICHAEL NAYAK
UU	UU	UU	NONE	11	19b. TELEPHONE NUMBER *(Include area code)* 808-891-7727

Reset

Optimal Guidance Trajectories for a Nanosat Docking with a Non-Cooperative Resident Space Object

Parv Patel
University of Southern California
Los Angeles, CA 90089
404-452-9090
parvpate@usc.edu

Bogdan Udrea
VisSidus Technologies Inc.
Daytona Beach, FL 32114
206-227-8075
bogdan.udrea@vissidus.com

Michael Nayak
Red Sky Research
Albuquerque, NM 87108
386-983-6135
nayak@redskyresearch.org

***Abstract*—There has been an increasing interest in on-orbit autonomous servicing and repair of satellites as well as controlled active debris removal (ADR) in the space industry recently. One of the most challenging tasks for servicing/repair as well as for ADR is the rendezvous and docking with a non-cooperative tumbling resident space object (RSO). This paper presents a propellant optimal maneuver profile for a servicing spacecraft to perform proximity operations and eventually dock with a non-cooperative target. The strategy is to find an optimal trajectory which will guide the servicing spacecraft to approach the tumbling satellite such that the two vehicles will eventually have no relative motion. Therefore, a subsequent docking or capture operation can be safely performed. The research described here elaborates on the previous work that studied the minimum-control-effort for a 3-D docking to a tumbling object considering a full six-degree-of-freedom model of both chaser and target. The current work expands the scope by adding new set of linearized equations of motion that capture the effect of the J_2 geopotential disturbance force.**

Typically, Hill's linearized equation of relative motion have been used for this analysis, but they fail to capture the effect of J_2 disturbance force on the chaser satellite. Firstly, the effects of the J_2 disturbance force is added to the linearized equations of motion by the addition of the J_2 terms. Secondly, minimum-control-effort optimality condition is examined and propellant optimal trajectories for a relative motion problem are then numerically solved, by using a direct collocation method based on the Gauss pseudospectral approach. The simulation results shows the effect of errors caused by the oblateness of the earth (as described by the J_2 potential) on the described relative motion problem. Furthermore, effect of J_2 disturbance on the optimal trajectory is discussed for the minimum propellant-consumption optimality condition.

TABLE OF CONTENTS

1. INTRODUCTION

There has been an increasing interest in satellite on-orbit autonomous servicing in the space industry recently. JAXA recently completed a technology demonstration mission ETS-7 [13]. NASA did an autonomous rendezvous mission through the Demonstration for Autonomous Rendezvous Technology (DART) in 2005 [8], where the mission was not completed due to more than expected propellant usage during rendezvous maneuvering. Air Force Research Laboratory's (AFRL) Experimental Satellite Systems-10 and 11 (XSS-10 and XSS-11) have been developed in order to show the ability for a small sat to autonomously plan and rendezvous with a passive and cooperative Resident Space Object (RSO) in Low Earth Orbit (LEO) [1]. In addition, Defense Advance Research Projects Agency's (DARPA) Orbital Express (OE) Advance Technology Demonstration Program validated the technology and techniques for on-orbit refueling and configuration of two satellites [3][4]. The existence of this programs demonstrates that there is a need for a robust and effective autonomous close proximity control algorithms for multiple spacecraft. The use of micro-satellites to inspect, service, repair, deorbit and refuel larger spacecrafts is a long-term goal.

In order to perform on-orbit service, the servicing spacecraft has to first rendezvous and dock with the satellite to be serviced in orbit. The tumbling of an uncontrolled resident space object (RSO) or the rotational and transnational motion of an non-cooperating RSO present challenges to the docking operations.

From a theoretical standpoint, the present paper elaborates on the previous work by Boyarko et al. [5][6][7], who studied the minimum-time and minimum-control problem for a rendezvous of a chaser satellite to a tumbling object considered a full six-degree-of-freedom model of both chaser and target. The current work expands the scope by adding the effect of J_2 geopotential disturbance force and investigates its effects on the proximity operations.

The majority of previous research pertaining to operations that focused on rendezvous with an uncontrolled RSO, the relative motion dynamics pertinent to proximity space operation only considers Hill's equations, also known as Clohessy-Wiltshire equations. The reason being Hill's equations are very simple to implement and have been successfully used to describe the relative motion of two satellite during rendezvous maneuvers. Although, the assumption made by Hill's equations that is cited repeatedly as the main source of error is that the Earth is perfectly spherical. Because the Earth is not perfectly spherical, but rather an oblate spheroid and the dominant term of the series expansion of this effect is the J_2 term, modeling errors are introduced by the noncentral forces. To reduce the effect of the modeling errors that are present in Hill's equations, much research has been done with varying success to incorporate the effects of the J_2 potential.

This papers implements the formulation of Schweighart and

978-1-4799-5380-6/15/$31.00 ©2015 IEEE.
[1] IEEEAC Paper #2199, Version 0.1, Updated 20/10/2014.

Sedwick [11][12] which describes the linear combination of Hill's equation with J_2 effect. The equations derived by Schweighart and Sedwick [11][12] provides insight into the relative motion of satellites under the influence of the J_2 potential. The period mismatch between the in-plane and cross-track motion produces an effect called tumbling in which the spacecraft formation appears to tumble around the orbital angular momentum vector. Additionally, small differences in the orbital inclination of the satellites in the formation cause differential drift in the longitude of the ascending node. This differential drift causes the spacecraft formation to break up over time. The paper is organized as follows. Section 2 presents the equations of relative motion that incorporate the effect of the J_2 perturbation. The analysis of the relative motion with Hill's equations and the derived time-averaged J_2 model with corrections along with the full J_2 effect is presented in Section 3. The set up of the optimization problem is presented in Section 4 and the results are presented and analyzed in Section 5.

2. Relative Motion Models

Figure [1] illustrates the curvilinear $\hat{\boldsymbol{x}}$ (radial) $\hat{\boldsymbol{y}}$ (along-track) $\hat{\boldsymbol{z}}$ (cross-track) axis system used for the problem. The $\hat{\boldsymbol{x}}$ vector points in the radial direction, the $\hat{\boldsymbol{z}}$ vector is perpendicular to the orbital plane and points in the direction of the angular momentum vector. Finally, the $\hat{\boldsymbol{y}}$ vector completes movement. In the $\hat{\boldsymbol{x}}$ - $\hat{\boldsymbol{y}}$ - $\hat{\boldsymbol{z}}$ coordinate system, the specification is made that it is a curvilinear coordinate system. The $\hat{\boldsymbol{x}}$ vector remains unchanged, however the $\hat{\boldsymbol{y}}$ and the $\hat{\boldsymbol{z}}$ vector 'curves' around the orbit.

Unlike the Local Vertical, Local Horizontal (LVLH) body fixed frame, implemented by the Hill's equations, the only difference comes from the fact that the LVLH frame is not defined as a curvilinear system but as a rectangular.

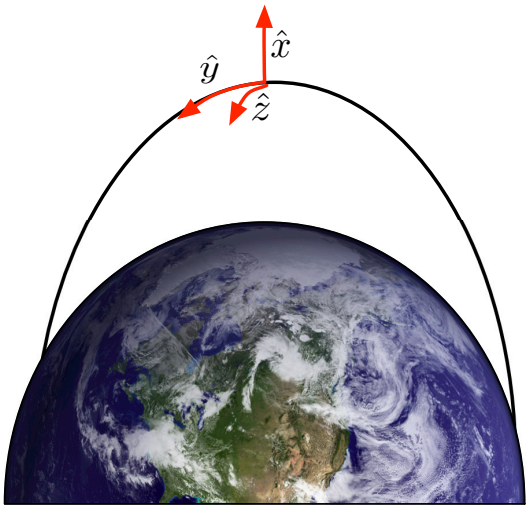

Figure 1. The $\hat{\boldsymbol{x}}$-$\hat{\boldsymbol{y}}$-$\hat{\boldsymbol{z}}$ Curvilinear Body-Fixed Coordinate System.

Figure [2] illustrates the $\hat{\boldsymbol{r}}$ - $\hat{\boldsymbol{\theta}}$ - $\hat{\boldsymbol{i}}$ spherical coordinate system used to describe the gravitational acceleration and the J_2 potential due to the spherical earth . The $\hat{\boldsymbol{r}}$ points in the radial direction, $\hat{\boldsymbol{i}}$ is the azimuthal angle measured around the line of nodes, and $\hat{\boldsymbol{\theta}}$ is the co-latitude measured from the ascending node which acts as the pole of the spherical system.

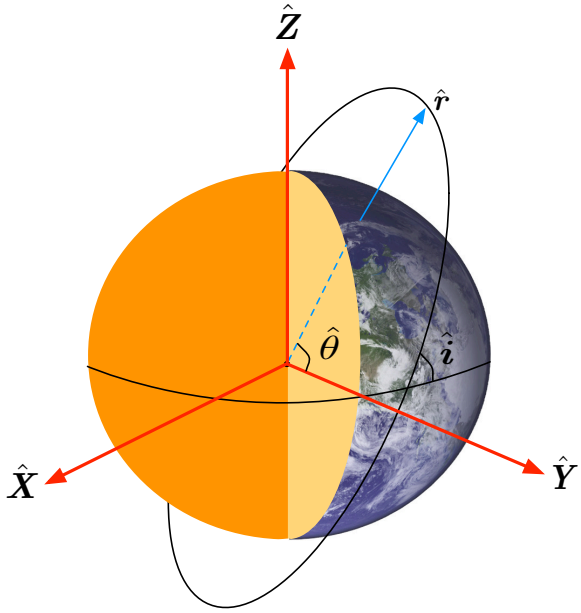

Figure 2. The $\hat{\boldsymbol{r}}$-$\hat{\boldsymbol{\theta}}$-$\hat{\boldsymbol{i}}$ Spherical Body-Fixed Coordinate System.

Conversion between both these body fixed coordinate systems is fairly straightforward. The radial vector in each coordinate system completely coincides. The $\hat{\boldsymbol{y}}$ vector, and $\hat{\boldsymbol{\theta}}$ coincide; and the $\hat{\boldsymbol{z}}$ vector and the $\hat{\boldsymbol{i}}$ vector coincide. In this way, the curviliniar coordinate system defined is very much like a spherical coordinate system.

A summary of the mathematical model development is performed and described below in order to highlight the set of equations of motion that are considered for the relative motion problem between a controlled satellite (Chaser) w.r.t to the assumed reference orbit (Non-Cooperative Target).

The derivation begins with the analytic equation of motion for an orbiting satellite under the influence of the J_2 potential.

$$\ddot{\boldsymbol{r}} = \boldsymbol{g}(\boldsymbol{r}) + \boldsymbol{J}_2(\boldsymbol{r}) \tag{1}$$

where, $\boldsymbol{g}(\boldsymbol{r})$ is the gravitational acceleration due to spherical Earth,

$$\boldsymbol{g}(\boldsymbol{r}) = -(\mu/r^2)\hat{\boldsymbol{r}} \tag{2}$$

$\boldsymbol{J}_2(\boldsymbol{r})$ is the acceleration due to J_2 potential [9],

$$\begin{aligned}\boldsymbol{J}_2(\boldsymbol{r}) = -(3/2)(J_2\mu R_e^2/r^4)[(1-3\sin^2 i\sin^2\theta)\hat{\boldsymbol{x}} \\ +(2\sin^2 i\sin\theta\cos\theta)\hat{\boldsymbol{y}} + (2\sin i\cos i\sin\theta)\hat{\boldsymbol{z}}]\end{aligned} \tag{3}$$

$\boldsymbol{r}$ is the position vector of the satellite, and $\hat{\boldsymbol{x}}$-$\hat{\boldsymbol{y}}$-$\hat{\boldsymbol{z}}$ is the coordinate system described in Figure [1].

The models are developed by considering the relative motion between one satellite and a reference orbit. For now, the derivation only requires that the reference orbit is constant radius (circular) and the equation of motion for the reference

$$\nabla \boldsymbol{J}_2(\boldsymbol{r}) = \frac{6\mu J_2 R_e^2}{r^5} \begin{bmatrix} (1 - 3\sin^2 i \sin^2\theta) & \sin^2 i \sin 2\theta & \sin 2i \sin 2\theta \\ \sin^2 i \sin 2\theta & -\frac{1}{2} - \sin^2 i(\frac{1}{2} - \frac{7}{4}\sin^2\theta) & -\frac{\sin 2i cos\theta}{4} \\ \sin 2i \sin\theta & -\frac{\sin 2i cos\theta}{4} & -\frac{3}{4} + \sin^2 i(\frac{1}{2} + \frac{5}{4}\sin^2\theta) \end{bmatrix} \tag{8}$$

orbit is given by the Newton's law of motion in a central force field:

$$\ddot{\boldsymbol{r}}_{\text{ref}} = \boldsymbol{g}(\boldsymbol{r}_{\text{ref}}) \tag{4}$$

Furthermore, linearizing the gravitational terms in Equation (1) with respect to the defined reference orbit results in

$$\ddot{\boldsymbol{r}} = \boldsymbol{g}(\boldsymbol{r}_{\text{ref}}) + \boldsymbol{g}(\boldsymbol{r}_{\text{ref}}) \cdot \boldsymbol{x} + \boldsymbol{J}_2(\boldsymbol{r}_{\text{ref}}) + \nabla \boldsymbol{J}_2(\boldsymbol{r}_{\text{ref}}) \cdot \boldsymbol{x} \tag{5}$$

where, the relative position of the satellite with respect to the reference orbit is given by $\boldsymbol{x}$ as represented in Figure [3]

$$\boldsymbol{x} = \boldsymbol{r} - \boldsymbol{r}_{\text{ref}} \tag{6}$$

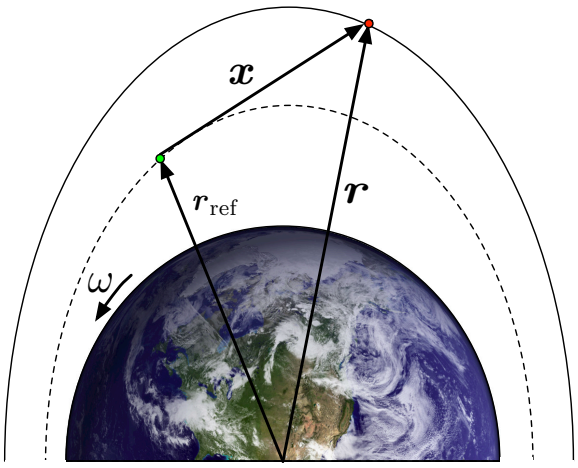

Figure 3. The Reference Orbit

When a spherical coordinate system ($\hat{\boldsymbol{r}}$ - $\hat{\boldsymbol{\theta}}$ - $\hat{\boldsymbol{i}}$) with the pole aligned with the ascending node is used, the gradient of the $\boldsymbol{g}(\boldsymbol{r})$ gravitational acceleration can be calculated. The result is:

$$\nabla \boldsymbol{g}(\boldsymbol{r}) = \begin{bmatrix} 2(\mu/r^3) & 0 & 0 \\ 0 & -(\mu/r^3) & 0 \\ 0 & 0 & -(\mu/r^3) \end{bmatrix} \tag{7}$$

The J_2 disturbance in Equation (3) is given in $\hat{\boldsymbol{x}}$ - $\hat{\boldsymbol{y}}$ - $\hat{\boldsymbol{z}}$ coordinates. However, the equation can be transformed directly to the $\hat{\boldsymbol{r}}$ - $\hat{\boldsymbol{\theta}}$ - $\hat{\boldsymbol{i}}$ coordinate system without any loss of generality. Taking the gradient gives Equation (8)

Because the reference frame is rotating, rotational terms are added when calculating the relative acceleration and velocities of the satellite w.r.t. the reference orbit.

$$\ddot{\boldsymbol{x}} = \ddot{\boldsymbol{r}} - \ddot{\boldsymbol{r}}_{\text{ref}} - 2\boldsymbol{\omega} \times \dot{\boldsymbol{x}} - \dot{\boldsymbol{\omega}} \times \boldsymbol{x} - \boldsymbol{\omega} \times (\boldsymbol{\omega} \times \boldsymbol{x}) \tag{9}$$

For a circular reference orbit the rotation rate of the coordinate system is constant given by

$$\boldsymbol{\omega} = n\hat{\boldsymbol{z}}, \qquad n = \sqrt{\mu / r_{ref}^3} \tag{10}$$

Substituting Equation (5) into Equation (9) and rearranging the terms gives us:

$$\begin{aligned} \ddot{\boldsymbol{x}} + 2\boldsymbol{\omega} \times \dot{\boldsymbol{x}} + \dot{\boldsymbol{\omega}} \times \boldsymbol{x} + \boldsymbol{\omega} \times (\boldsymbol{\omega} \times \boldsymbol{x}) = \boldsymbol{g}(\boldsymbol{r}_{\text{ref}}) \\ + \boldsymbol{g}(\boldsymbol{r}_{\text{ref}}) \cdot \boldsymbol{x} + \boldsymbol{J}_2(\boldsymbol{r}_{\text{ref}}) + \nabla \boldsymbol{J}_2(\boldsymbol{r}_{\text{ref}}) \cdot \boldsymbol{x} - \ddot{\boldsymbol{r}}_{\text{ref}} \end{aligned} \tag{11}$$

The equation above can be further simplified by canceling out $\boldsymbol{g}(\boldsymbol{r}_{\text{ref}})$ with $\ddot{\boldsymbol{r}}_{\text{ref}}$ as they are equal as seen in equation (4). In the following sections the above equation along with Hill's Eqn. are presented as a comparison to the time averaged J_2 equations, with reference orbit period and nodal drift corrections. These time averaged J_2 equations with corrections are derived in the following subsections below.

Time Averaged ∇J_2

Equation (11) is a linearized differential equation of motion with time varying coefficients. The ODE with time varying coefficient in Equation (11) is cast into an ODE with time varying coefficient by taking the time average of the ∇J_2 term

$$\frac{1}{2\pi} \int_0^{2\pi} \nabla \boldsymbol{J}_2(\boldsymbol{r}) d\theta = \frac{\mu}{r^3} \begin{bmatrix} 4s & 0 & 0 \\ 0 & -s & 0 \\ 0 & 0 & -3s \end{bmatrix} \tag{12}$$

where,

$$s = (3J_2 R_e^2 / 8r^2)(1 + 3\cos 2i) \tag{13}$$

Adding the time-averaged term and removing $\boldsymbol{g}(\boldsymbol{r}_{\text{ref}})$ with $\ddot{\boldsymbol{r}}_{\text{ref}}$ Equation (11) becomes,

$$\begin{aligned} \ddot{\boldsymbol{x}} + 2\boldsymbol{\omega} \times \dot{\boldsymbol{x}} + \dot{\boldsymbol{\omega}} \times \boldsymbol{x} + \boldsymbol{\omega} \times (\boldsymbol{\omega} \times \boldsymbol{x}) = \boldsymbol{g}(\boldsymbol{r}_{\text{ref}}) \cdot \boldsymbol{x} \\ + \boldsymbol{J}_2(\boldsymbol{r}_{\text{ref}}) + \frac{1}{2\pi} \int_0^{2\pi} \nabla \boldsymbol{J}_2(\boldsymbol{r}_{\text{ref}}) \cdot \boldsymbol{x} d\theta \end{aligned} \tag{14}$$

By adding the time average of the gradient of the J_2 disturbance, the periodic component of the gradient is lost. As the values of $\boldsymbol{g}(\boldsymbol{r}_{\text{ref}})$ and $\boldsymbol{J}_2(\boldsymbol{r}_{\text{ref}})$ and the gradients of these terms

are evaluated at the reference orbit, $\boldsymbol{x}$ must remain relatively small for the the first order term of the Taylor series expansion that is used in the derivation of the equations of motion to apply and therefore, the mean radii and orbital rates of the perturbed satellite and reference satellite must be similar.

Effect of the J_2 perturbation also causes a drift in the longitude of ascending node which varies with inclination. The J_2 perturbed satellite will experience this drift, but the reference orbit will not, thus the two orbits will gradually separate unless some correction to the orbital rate and nodal drift of the reference satellite is included in the model.

The fact that the ∇J_2 term has been time averaged over a period in Equation (14) has the effect to cause errors in cross-track motion. It is seen that cross-track motion is due solely to that the satellite's orbit and the associated reference are not coplaner. It is a periodic motion that is equal to zero when the two orbital planes intersect and is at a maximum 90° away from the intersection of the planes. As this paper deals with docking application focusing where the satellite is in close vicinity with the reference orbit, both having similar inclinations, effects to the cross-track errors are not accounted in this paper. Although addition and studying the effect of these cross track errors will be a topic explored in future.

Correcting the orbital period of the reference orbit

Under the influence of the J_2 disturbance, the perturbed satellite will have a different orbital period than when unperturbed. Because of this discrepancy, the perturbed satellite drifts from the unperturbed reference orbit and eventually the linearized equations break down. To fix this problem, the period of the reference orbit must be adjusted to match the period of the satellites in the cluster.

The change in period due to the J_2 disturbance as given by Schweighart and Sedwick can be found from the average J_2 disturbance (not to be confused with the time average of the gradient of the J_2 term taken above). The equation of motion of the reference orbit, as seen in Equation (4), now becomes,

$$\ddot{\boldsymbol{r}}_{\text{ref}} = \boldsymbol{g}(\boldsymbol{r}_{\text{ref}}) + \frac{1}{2\pi}\int_0^{2\pi} \boldsymbol{J}_2(\boldsymbol{r}_{\text{ref}})d\theta \tag{15}$$

where the time averaged J_2 acceleration is given by Eq. (16) below,

$$\frac{1}{2\pi}\int_0^{2\pi} \boldsymbol{J}_2(\boldsymbol{r})d\theta = \begin{bmatrix} -n^2 rs \\ 0 \\ 0 \end{bmatrix} \tag{16}$$

This results in a non-zero value for acceleration in the radial $\hat{\boldsymbol{x}}$ direction only. This can be visualized as an additional force acting to increase the Keplerian gravity term. Therefore, if a satellite is to remain in a circular orbit its orbital rate must be increased above that for Keplerian dynamics.

Substituting Equation (15) in Equation (11), we get

$$\begin{aligned}\ddot{\boldsymbol{x}} + 2\boldsymbol{\omega}\times\dot{\boldsymbol{x}} + \dot{\boldsymbol{\omega}}\times\boldsymbol{x} + \boldsymbol{\omega}\times(\boldsymbol{\omega}\times\boldsymbol{x}) &= \boldsymbol{g}(\boldsymbol{r}_{\text{ref}})\cdot\boldsymbol{x} + \boldsymbol{J}_2(\boldsymbol{r}_{\text{ref}}) \\ &+ \frac{1}{2\pi}\int_0^{2\pi}\nabla\boldsymbol{J}_2(\boldsymbol{r}_{\text{ref}})d\theta\cdot\boldsymbol{x} - \frac{1}{2\pi}\int_0^{2\pi}\boldsymbol{J}_2(\boldsymbol{r}_{\text{ref}})d\theta\end{aligned} \tag{17}$$

As the rate of the reference orbit has changed, so has the average angular speed of the reference satellite, and the coordinate system which is based there. The new angular velocity can be found by equating the accelerations to give

$$\boldsymbol{\omega} = nc\hat{\boldsymbol{z}}, \qquad c = \sqrt{1+s} \tag{18}$$

where "s" in Equation (15) and Equation (17) is given by,

$$s = \frac{3J_2R_e^2}{8r^2}(1+\cos 2i) \tag{19}$$

Correcting the Reference Orbit for Nodal Drift

Although the preceding equations of motion are a vast improvement over Hill's equations when incorporating the J_2 disturbance, more can be done. Even though the orbital period of the reference orbit has been adjusted to match the period of the satellite under the influence of the J_2 potential, they still drift apart due to separation of the longitude of the ascending node. Schweighart and Sedwick worked out analytically a separation distance between the perturbed satellite and the reference orbit as $\boldsymbol{r}_{\text{ref}}\triangle\Omega\sin i$ over one period. Similarly, after two orbital periods, the satellite and the reference orbit will be separated by $\boldsymbol{r}_{\text{ref}}2\triangle\Omega\sin i$, and this process will continue to cause them to drift farther and farther apart. Although the equations of motion in their current form do capture the bulk of this motion, the increasing separation causes the linearization to break down after several periods. Because of this, the reference orbit must again be redesigned so that it tracks this secular motion.

This separation in longitude of ascending node as given by Schweighart and Sedwick, shows that only the normal component of the J_2 acceleration is responsible for the drift. Applying the normal component of the J_2 disturbance acceleration to the updated reference orbit [Equation (15)] gives us:

$$\ddot{\boldsymbol{r}}_{\text{ref}} = \boldsymbol{g}(\boldsymbol{r}_{\text{ref}}) + \frac{1}{2\pi}\int_0^{2\pi}\boldsymbol{J}_2(\boldsymbol{r}_{\text{ref}})d\theta + [\boldsymbol{J}_2(\boldsymbol{r}_{\text{ref}})\cdot\hat{\boldsymbol{z}}]\hat{\boldsymbol{z}} \tag{20}$$

Time-Averaged J_2 EQM with Corrections

The final equation of motion which captures the effect of J_2 disturbance alonga with reference orbit period and nodal drift corrections is described below. As we added a component of the J_2 potential to the reference orbit for the correction of nodal drift, that component must be subtracted from the equations of motion of the satellite relative to the reference orbit [Equation (17)]. The resulting equations of motion in vector for are:

$$\begin{aligned}\ddot{\boldsymbol{x}} + 2\boldsymbol{\omega}\times\dot{\boldsymbol{x}} + \dot{\boldsymbol{\omega}}\times\boldsymbol{x} + \boldsymbol{\omega}\times(\boldsymbol{\omega}\times\boldsymbol{x}) &= \boldsymbol{g}(\boldsymbol{r}_{\text{ref}})\cdot\boldsymbol{x} \\ &+ \boldsymbol{J}_2(\boldsymbol{r}_{\text{ref}}) + \frac{1}{2\pi}\int_0^{2\pi}\nabla\boldsymbol{J}_2(\boldsymbol{r}_{\text{ref}})d\theta\cdot\boldsymbol{x} \\ &- \frac{1}{2\pi}\int_0^{2\pi}\boldsymbol{J}_2(\boldsymbol{r}_{\text{ref}})d\theta - [\boldsymbol{J}_2(\boldsymbol{r}_{\text{ref}})\cdot\hat{\boldsymbol{z}}]\hat{\boldsymbol{z}}\end{aligned} \tag{21}$$

The above equations can be expanded by substituting the appropriate terms results in a set of differential equations of form,

$$\ddot{x} - 2(nc)\dot{y} - (5c^2 - 2)n^2 x = -3n^2 J_2 (R_e^2/r_{\text{ref}}) \times [\tfrac{1}{2} - 3\sin^2 r_{\text{ref}} \sin^2(kt)/2 - (1 + \cos 2i_{\text{ref}})/8]$$

$$\ddot{y} + 2(nc)\dot{x} = -3n^2 J_2 (R_e^2/2r_{\text{ref}}) \sin^2 i_{\text{ref}} \sin(2kt) \tag{22}$$

$$\ddot{z} + (3c^2 - 2)n^2 z = 0$$

where k is defined as,

$$k = nc + \frac{3\sqrt{\mu} J_2 R_e^2}{2r^{7/2}} \cos^2 i \tag{23}$$

The above differential equations are used for solving the optimal control problem described in this paper. Prior to setting up the simulation, the section below goes over the effect of J_2, with and without corrections as compared to Hill's equation, to highlight the motivation of this study and understand the effect of the errors on the relative position of the perturbed satellite.

3. Effects of J_2 Disturbance

This section highlights the effect of J_2 perturbations on the relative motion of the perturbed satellite with respect to the reference orbit. Moreover, error related to reference orbital period and nodal drift are highlighted. Finally, the effect of disturbance of J_2 potential is studied in comparison to Hill's equation of motion.

Numerical simulations are performed using fixed-step `ODE5` integrator to plot relative motion trajectories. The orbital parameters chosen for the reference orbit where the target is placed are: $i_{\text{ref}} = 70°$, the apogee and perigee altitude is given by $r_a = 919$-km and $r_p = 902$-km respectively. The rationale for choosing the above orbital parameters is discussed in Sec. 4 where the optimization problem for this study is formulated.

The following Figure [4] demonstrates the effect of the J_2 geopotential disturbances at 70° inclination. The purpose to acquire the J_2 effect on the chaser from both the equatorial and polar regions, a logical choice of starting from [-1, 0, 0] km is employed as the initial condition for the relative position, thus in order to attempt to only simulate the J_2 effect on the pure in-track motion. The chaser is assumed to be at rest initially. All the simulations below for this section are propagated for the time span of two orbital period of the reference orbit which comes to 3.44 hrs.

It is seen in Figure [4] the considerable relative position error created by the J_2 disturbance and the importance for its implementation while studying the optimal trajectory design for rendezvous and proximity operations. Additionally, it is noted that the J_2 model without corrections corresponding to Equation (11) adds sizable cross-track errors as a result of orbital period mismatch between the target and the chaser orbits and, the nodal drift caused by the separation of the longitude of the ascending node.

The relative position errors between the commonly used Hill's equations and the time-averaged J_2 with corrections model is shown in Figure [5]. As seen in the figure, the

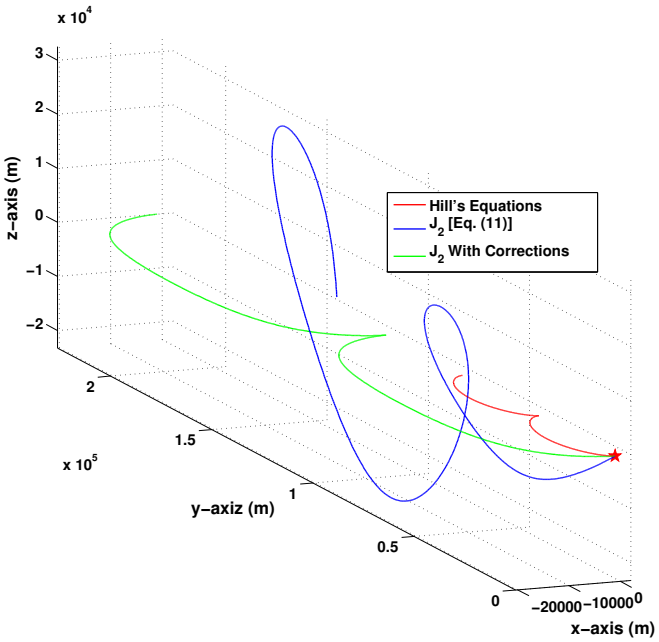

Figure 4. Relative motion trajectories ($i_{\text{ref}} = 70°$).

error in the in-track motion ($\hat{\mathbf{x}}$) tops out at ~ 15 km and error propagation in time looks periodic. Similarly, for the radial motion ($\hat{\mathbf{y}}$) the error due to the J_2 seems to be increasing sharply with time. Finally, for the cross-track motion ($\hat{\mathbf{z}}$) even though the error is not significant compared to in-track and radial motion, the profile shows an increasing deviation with time. With periodic errors in the in-tack motion and the increasing errors in both the radial and cross-track direction, a significant effect of J_2 perturbation on the chaser is seen.

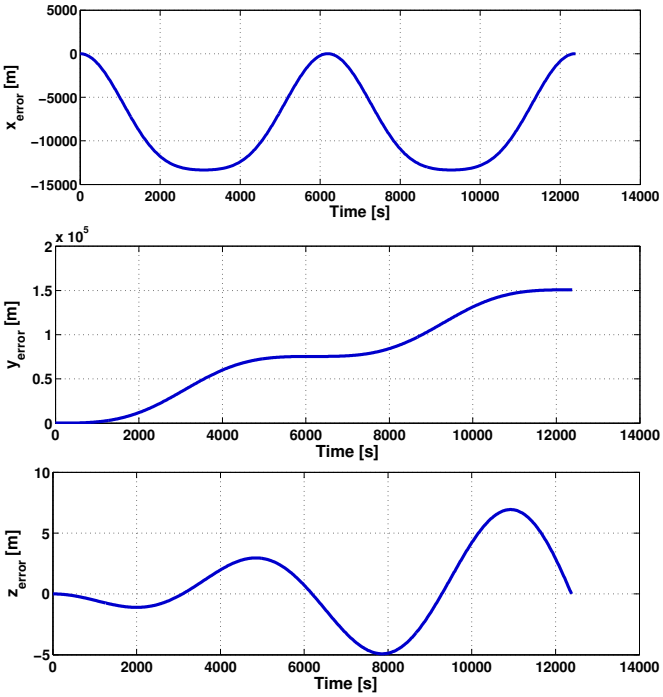

Figure 5. Relative position errors between Hill's Eqns. and Time-averaged J_2 with corrections Eqns. ($i_{\text{ref}} = 70°$).

Figure [6] presents similar relative position errors between the time-averaged J_2 model with corrections and, the J_2 equations without any corrections [Equation (11)] to highlight the effect caused by the orbital period mismatch and the separation in the ascending node causing the nodal drift. As expected, the position error in all three directions is significant. As a consequence, the implementation of the corrections is crucial for studying the optimal trajectory design for proximity applications. Moreover when compared to Figure [5], it is seen that the implementation of the corrections reduces error in the $\hat{\mathbf{z}}$ direction which causes the motion of the chaser to create heavy cross-track deviations from the nominal as seen in Figure [4].

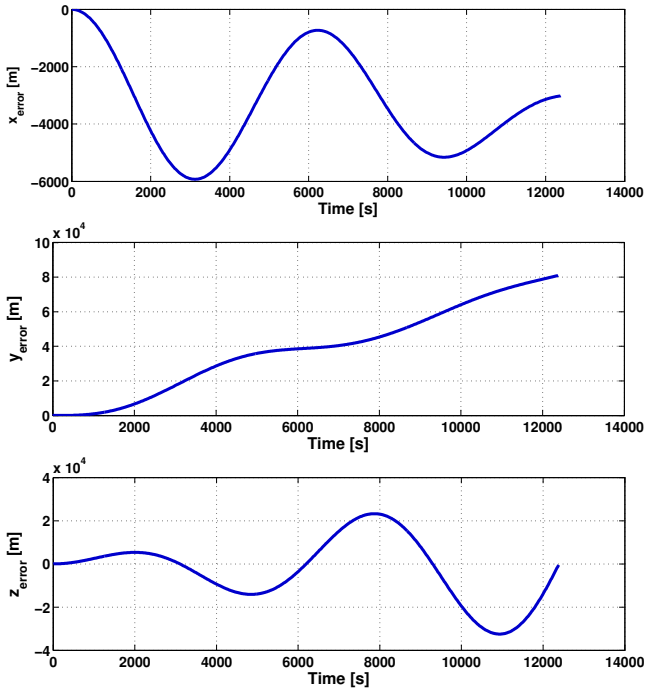

Figure 6. Relative position errors between Time-averaged J_2 with corrections Eqns. and J_2 without corrections Eqns. [Eqn. (11)] ($i_{\text{ref}} = 70°$).

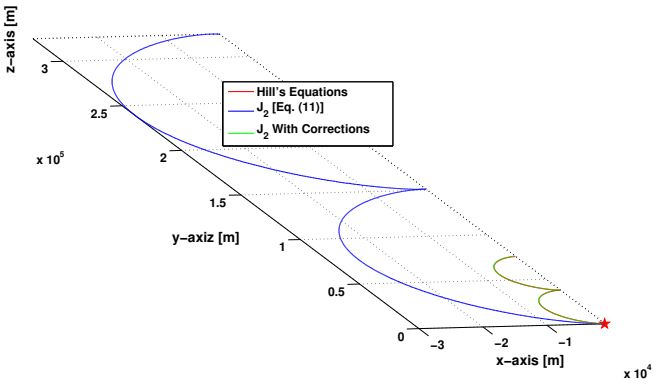

Figure 7. Relative motion trajectories ($i_{\text{ref}} = 0°$).

An interesting study would be to analyze the same three models at $0°$ inclination to validate the physics of the derived equations. Figure [7] shows the relative motion trajectories under the influence of the J_2 disturbance force. Is is seen that the relative motion of the chaser under the time-averaged J_2 with corrections model resembles with that of Hill's equations, as logically there would not be any effect of J_2 across the equator. Although a significant error is seen in the relative position given by the J_2 equations without corrections.

Figure [8] and Figure [9] illustrates the errors in the relative position of the spacecrafts between J_2 model with corrections with Hill's Equations and J_2 model without corrections [Equation (11)] respectively.

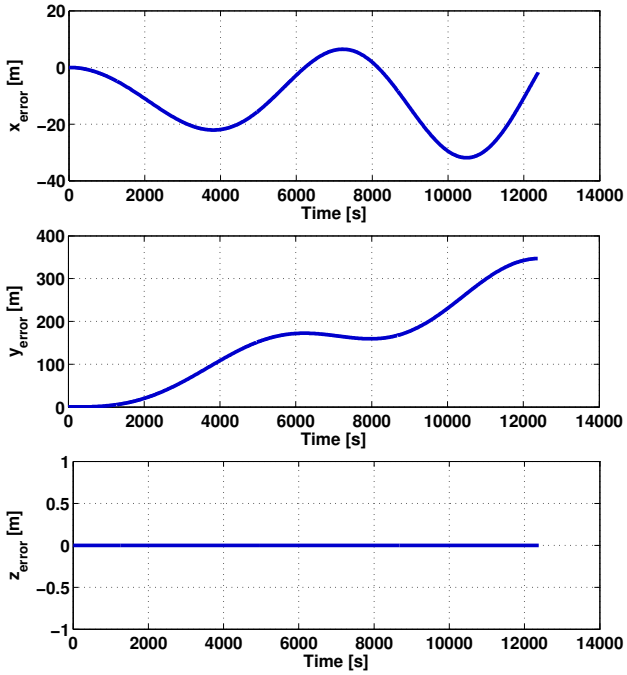

Figure 8. Relative position errors between Hill's Eqns. and Time-averaged J_2 with corrections Eqns. ($i_{\text{ref}} = 0°$).

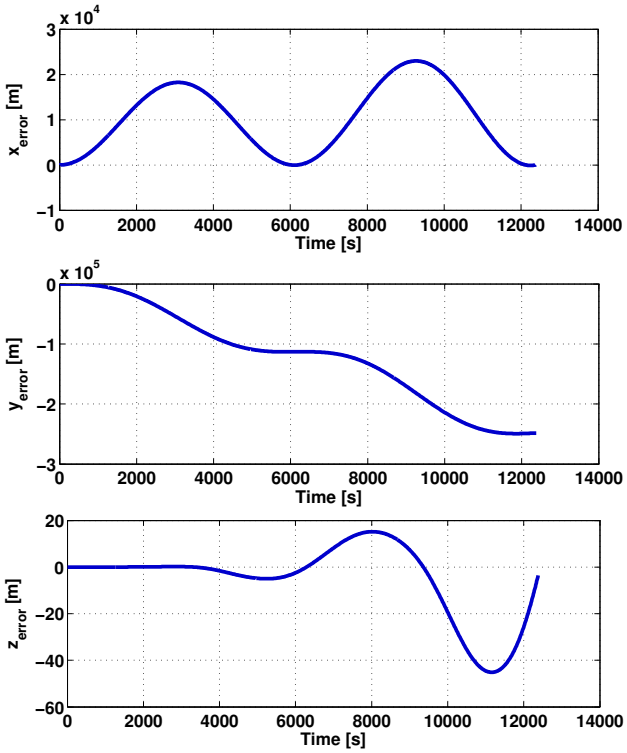

Figure 9. Relative position errors between Time-averaged J_2 corrections Eqns. and J_2 without corrections Eqns. [Eqn. (11)] ($i_{\text{ref}} = 0°$).

Figure [8] shows that the position errors between J_2 corrections model with Hill's equation are very small. The insignificant error noticed corresponds to the curvilinear coordinated system used for the derivation of the time-averaged J_2 equations. Validating the time-averaged J_2 corrections model once again at 0° inclination proves that the model used for the optimization problem formulation in the following section is a generalized case of Hill's Equation with J_2 perturbation incorporated in it.

Figure [9] further shows the inability of the full J_2 model without correction [Equation (11)] to fully capture the orbital period mismatch and nodal drifts errors. As expected the position errors in all three directions are significant.

From the study conducted in this section we see the importance of implementation of J_2 in the linear equations of relative motion for the study of the optimization operations.

4. OPTIMIZATION PROBLEM FORMULATION

This section develops a model of target-chaser rendezvous. The curvilinear coordinate system described in Section 2 is used for the model formation. We start from the arbitrary relative position and would like to bring the two spacecraft together for docking.

Using the notations described in the beginning of this paper based on the above model, the dynamics of the two system can now be described as follow. The translational kinematics and dynamics of a chaser spacecraft in the orbit frame centered at the target vehicle are given by Equation (21),

$$\begin{aligned}
\ddot{x} &= 2(nc)\dot{y} + (5c^2 - 2)n^2 x - 3n^2 J_2 (R_e^2/r_{\text{ref}}) \\
&\quad \times [\tfrac{1}{2} - 3\sin^2 r_{\text{ref}} \sin^2(kt)/2 - (1 + \cos 2i_{\text{ref}})/8] + f_x \\
\ddot{y} &= -2(nc)\dot{x} - 3n^2 J_2 (R_e^2/2r_{\text{ref}}) \sin^2 i_{\text{ref}} \sin(2kt) + f_y \\
\ddot{z} &= -(3c^2 - 2)n^2 z + f_z
\end{aligned} \tag{24}$$

where f_x, f_y and f_z are applied forces (controls) expressed in the Hill's frame.

Equation (24) hence defines a 6-state system of differential equations of relative motion governing the docking problem dynamics. Combined into the state vector $\mathbf{X}$ these states are,

$$\mathbf{X} = [x, y, z, \dot{x}, \dot{y}, \dot{z}] \tag{25}$$

The governing dynamics assumes three normalized controls:

$$\mathbf{u} = \left[\frac{f_x}{f_{xmax}} \quad \frac{f_y}{f_{ymax}} \quad \frac{f_z}{f_{zmax}} \right] \tag{26}$$

For simplicity, it is assumed that $f_{imax} = 1\text{m/s}^2$ for $i = x, y, z$. Once again, these controls are three normalized components of a translational force acting on a chaser f_i $(i = x, y, z)$, expressed in Hill's coordinate frame. All three controls are bounded: $\mathbf{u_{min}} \leq \mathbf{u} \leq \mathbf{u_{max}}$. The details of the thrust bounds are discussed in the subsection along with chaser mass and its thrust parameters.

Using the controls the two spacecrafts are brought together from some initial condition, given by 6 initial value of states $x_i(t_0),\ i = 1, ..., 6$ to docking conditions described by a final state, which for this problem is assumed to be a null i.e. $\mathbf{X}_f = \mathbf{O}$.

The goal of the optimization problem is to minimize propellant consumption during a maneuver of finite time of duration t_f. The objective function is then:

$$J(\mathbf{u}) = \int_0^{t_f} (\mid u_1(t) \mid + \mid u_2(t) \mid + \mid u_3(t) \mid) dt \tag{27}$$

Optimization Problem Setup

A sample maneuvering scenario is considered with the chaser center of mass starting at a distance of 1 km behind, 1 km below, and 1 km sideways from the target center of mass. Hence the initial values of the state for computer simulations discussed in the following sections is:

$$\mathbf{X}_0 = [-1000, -1000, -1000, 0, 0, 0]$$

The problem is further simplified by neglecting the geometrical structure of the both chaser and target. For the time being the final state is at the CoM of the target and with null relative velocity vector.

$$\mathbf{X}_f = [0, 0, 0, 0, 0, 0]$$

Baseline parameters are selected from a proposed controlled active debris removal (ADR) mission Curimba by Udrea and Nayak [14]. The authors describes Agena-D RBs as one of the potential target for the mission. Hence, the orbital parameters for this upper stage debri corresponds to the reference orbit chosen for this problem. As most of the Agena-D RBs are populated at approximately 70° the reference inclination for this problem is assumed 70°. Additionally, the apogee and the perigee altitude selected for the reference orbit where our target spacecraft is placed resembles that of the Agena-D RB which corresponds to $r_a = 919$ km and $r_p = 902$ km respectively. Furthermore, a time constraint is added to the simulation by fixing the final time to one-orbital period of the reference orbit, as for the ADR mission it requires the chaser to rendezvous with the target with the shortest amount of time.

The mission proposes a preliminary design of the chaser by considering a 12U CubeSat. This CubeSat is a three-axis stabilized spacecraft of 240×240×360 mm and a mass of 24 kg. It is known that the CubeSat has a miniaturized system consisting of 16 solenoid-fed thrusters placed such that they generate positive and negative torques about all three body axes with dual redundancy. The thruster arrangement also generates positive and negative forces about two of the three body axes. For the purpose of this work it has been assumed that the force along the third body axis is available when required. Future research will include constraints on the generation of force about the third body axis to take into account the finite slew time.

It is known from the preliminary design provided by the authors that the propellant used will be 1,1- difluorethane which can generate about 70 s of specific impulse. As for the first mission design iteration they assumed that each thruster

produces 50 mN of thrust force [14]. Knowing now the thrust force for individual thrusters (50 mN) and the chaser mass (24 kg), control bounds can be calculated for the optimal problem for the Equation (26). By these means the control bounds thus will be calculated by $\pm \mathbf{F_T}/\mathbf{m_{chaser}}$, where $\mathbf{F_T}$ is the total thrust produced by the chaser spacecraft thrusters. Solving for the control bounds for the defined rendezvous scenario and the assumed chaser parameters gives us: $-8.33\ \text{mm/s}^2 \leq \mathbf{u} \leq 8.33\ \text{mm/s}^2$

The above described optimal control problem is solved numerically, by the Gauss Pseudospectral Optimization Solver (GPOPS) [10]. The GPOPS is an open source code that implements a direct collocation method based on the Gauss Pseudospectral approach for solving optimal control problems.

Propellant-optimal trajectories are simulated with time-averaged J_2 with corrections model. To validate the correctness of the derived time-averaged J_2 equations, the trajectories with 0° inclination are simulated and compared with Hill's equations along with its control profiles. It should be seen that for this specific test condition, the optimal trajectories in both case should be perfectly similar along with its trust profile. Moreover, the effects of the correction errors on the optimal trajectories is also shown. The simulation results obtained including the optimal control profiles are discussed below.

5. Simulation Results

The minimum-propellant-control solution with the optimal controls defined in Equation (24) is here presented first. Additionally, the effect of the optimal trajectories with respect to the inclination is discussed, it also shows the effect of J_2 at different inclinations and how the optimal trajectories are influenced by it. Moreover, Equation (11) which incorporates only the differential J_2 without corrections is studied to see how the change in the reference orbital period and nodal drift errors affect the optimal solution. Finally, optimization results obtained with Hill's equations only are presented and compared.

Minimum Solution for Defined Rendezvous Scenario

For the minimum-propellant-control rendezvous scenario set in Section 4 the pseudospectral method yields the solution shown in Figure [10]. Additional planar views of the optimal trajectory is shown is figure [11].

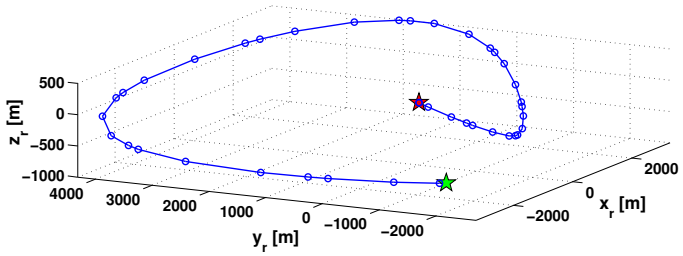

Figure 10. Optimal trajectory for time-averaged J_2 with corrections model ($i_{\text{ref}} = 70^\circ$).

The green marker shows the initial position of the chaser with respect to the target. The final maneuver time as discussed in the previous section is fixed at one orbital period of the reference orbit which when calculated comes to t_f = 1.72 hr and ends at the red marker. It is to be noted that the blue markers on the trajectory are the points where the thrust is applied and it is assumed that the thrust applied is impulsively.

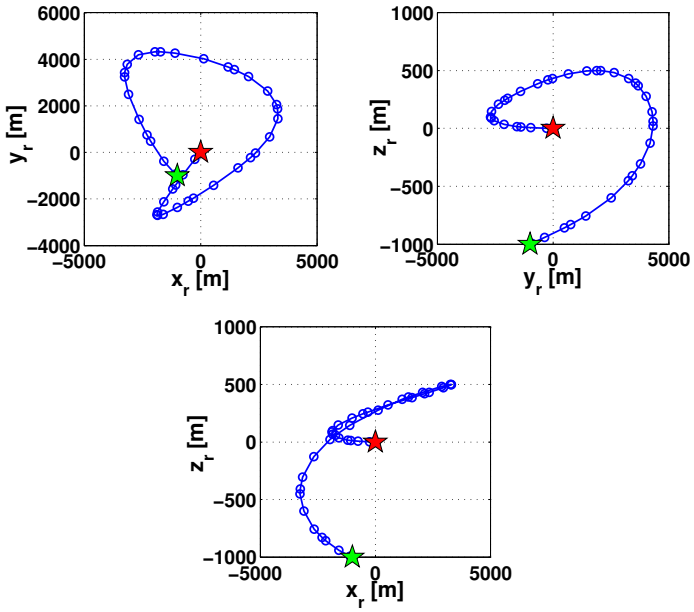

Figure 11. Planar view of the optimal trajectory for time-averaged J_2 with corrections model ($i_{\text{ref}} = 70^\circ$).

Figure [12] and Figure [13] shows the time history of the relative position and velocity of the optimal trajectory respectively. Along with that, the control profile for the three normalized components of the thrust force is displayed in Figure [14]. It is clearly seen that as there is no significant cross-track motion, the f_z control is not very active. On the other hand because of the large amplitude of the motion in the radial direction ($\dot{\mathbf{y}}$) and the two rapid consequential change in the radial directions makes the f_y control very active as it maxes out on the thrust bounds.

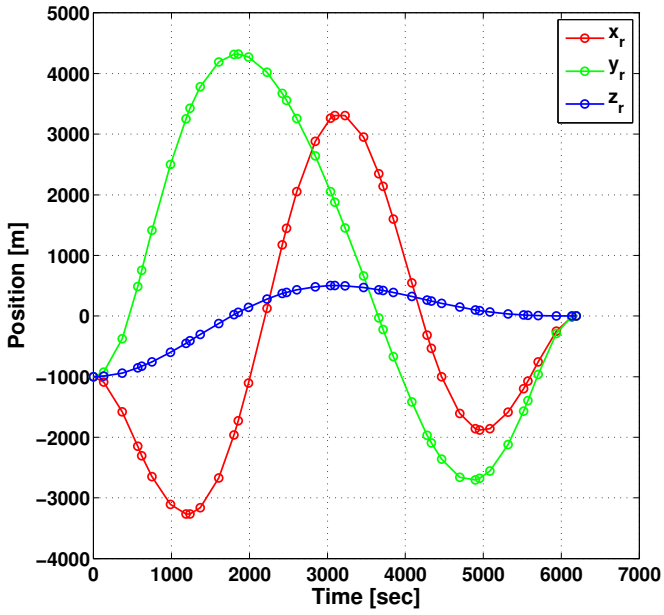

Figure 12. Position profiles for time-averaged J_2 with corrections model ($i_{\text{ref}} = 70^\circ$).

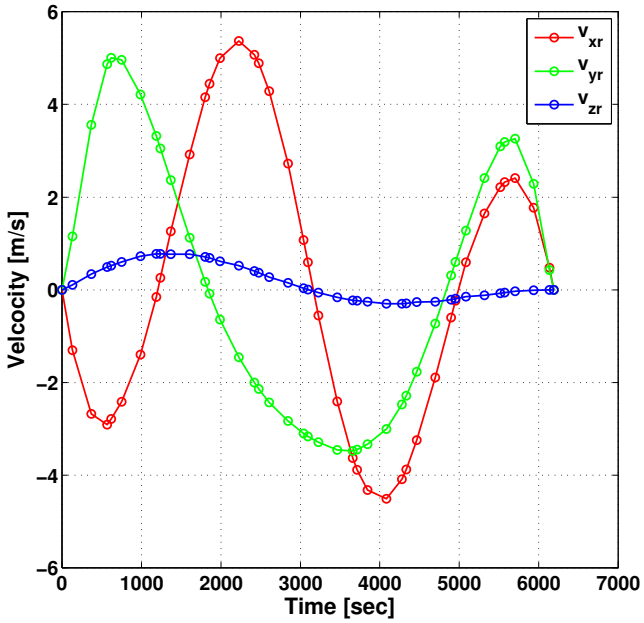

Figure 13. Velocity profiles for time-averaged J_2 with corrections model ($i_{\text{ref}} = 70°$).

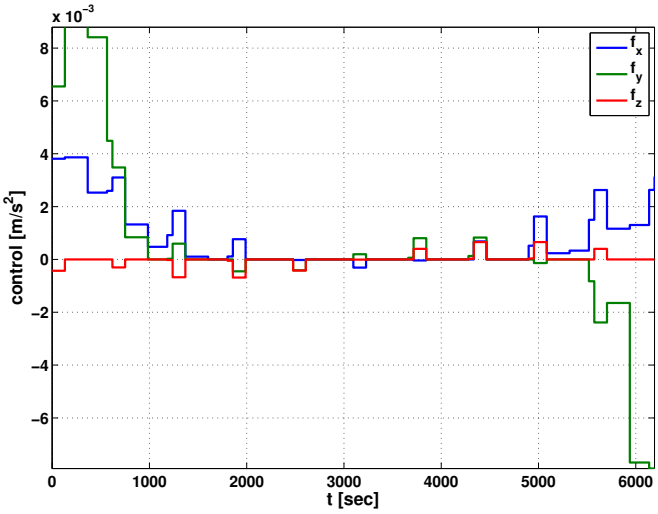

Figure 14. Minimum propellant control profiles for time-averaged J_2 with corrections model ($i_{\text{ref}} = 70°$).

It should be noted that the relative tolerance of 10^{-3} was set to solve the differential equations. Addition to that the terminal tolerance of the order of 10^{-6} is set for the NLP solved by GPOPS, which does not necessarily indicate the quality of the solution. The reason is that for the solution the parameters of the trajectory are only being computed at 41 nodes only where the optimality conditions are enforced.

For the implementation of the Gauss Pseudospectral method using GPOPS-II the guess for the initial states corresponds to the initial conditions and the guess for the final state consisted of zeros for the entire state. The guess for the control history was zero at the initial and final times for all controls. The solution obtained appears to be feasible but can be used only for offline computations, i.e. on an open-loop guidance scheme.

Minimum Propellant Solution for Hill's Equation

This sections draws differences in the optimality between the Hill's Equations and the time-averaged J_2 with corrections equation. The following figure shows the optimal trajectory for the Hill's equations. As expected a solution similar to Hohmann transfer is achieved. It can be hereby seen that the use of the Hill's equations for the study of optimal trajectories for rendezvous and proximity operations presents very conservative results.

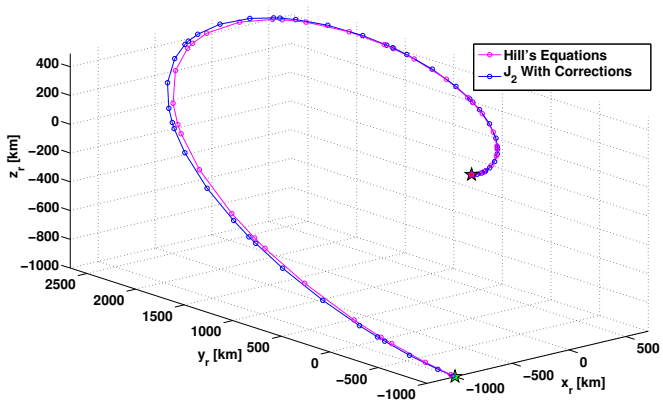

Figure 15. Optimal trajectory for the Hill's Equation and time-averaged J_2 with corrections ($i_{ref} = 0°$).

The above Figure [15] shows the propellant-optimal trajectories of the time-averaged J_2 with correction model for $0°$ inclination along with the the linearized Hill's equations of motion. Comparing the plotted optimal trajectories validates the correctness of the derived time-averaged J_2 correction equations. An insignificant error noticed in the relative position is in the same order of magnitude as seen in Figure [8] corresponding to the curvilinear coordinated system used for the derivation of the time-averaged J_2 equations.

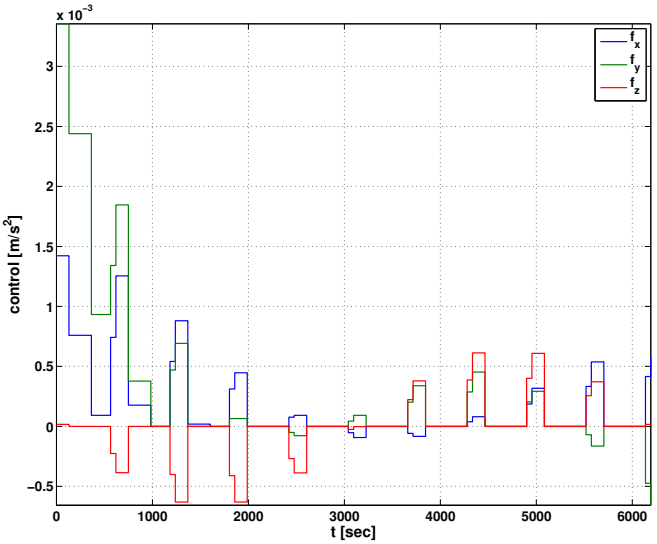

Figure 16. Minimum propellant control profiles for the Hill's Equation.

Figure [16] and Figure [17] shows a plot of the resulting control history of the three applied thrust forces corresponding to the optimal trajectory shown in Figure [15] using the linearized Hill's equations of motion and the time-averaged

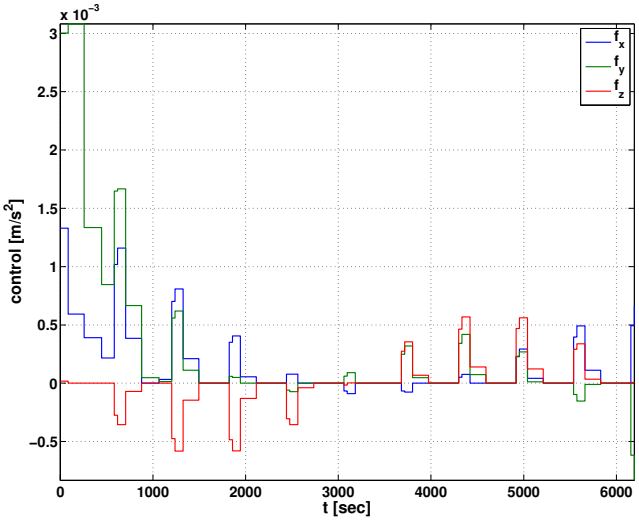

Figure 17. Minimum propellant control profiles for the time-averaged J_2 with corrections model ($i_{\text{ref}} = 0°$).

J_2 with corrections model for $0°$ inclination. Comparing the identical thrust profiles furthermore validates the correctness of the derived time-averaged J_2 equation used for this study.

Figure [18] adds to the study by showing the effect of the differential J_2 model without corrections for $70°$ inclination on the optimal trajectory profile. This simulated orbit is alongside plotted with optimal trajectories of the time-averaged J_2 with corrections model ($i_{ref} = 70°$) and the Hill's equations so as to fully understand the sizable errors in the optimal positions caused by the the orbital period mismatch between the target and the chaser orbits and the nodal drift caused by the separation of the ascending node.

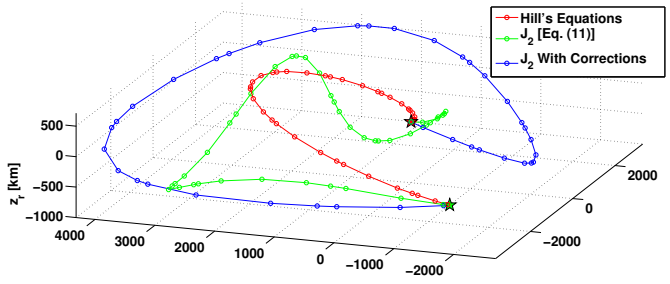

Figure 18. Optimal guidance trajectory for different models ($i_{ref} = 70°$)

Effect of Inclination on the Perturbed Optimal Trajectory

As the effect of J_2 potential is directly proportional to the inclination of the target of the reference orbit. A generalized plot below in Figure [19] that shows the J_2 perturbation effect on the optimal trajectories as the inclination of the reference orbit is increased.

It is seen that at lower inclinations the optimal route of the chaser is very similar to that of the Hill's equation as seen in Figure [15], which should be the case as we already discussed that the effect of J_2 is not very significant at inclinations near to equator ($0°$). For all the simulation plotted in Figure [19], the same rendezvous scenario is considered with fixed final maneuver time of one orbital period.

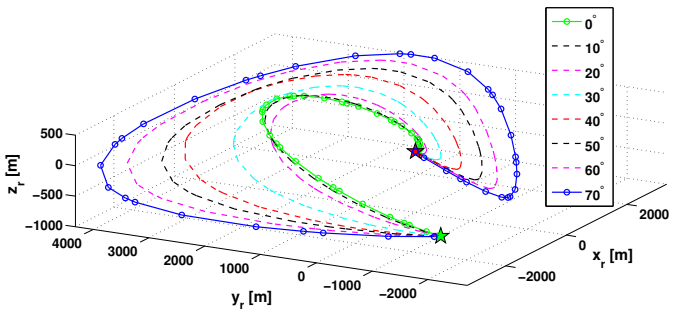

Figure 19. Optimal trajectory for time-averaged J_2 with corrections model for different inclination.

6. Conclusion

In this paper, the optimal close range rendezvous problem for a ADR spacecraft to approach a tumbling upper stage for capture is formulated and analyzed. A set of new linearized differential equations have been incorporated for describing the relative motion of satellites in the presence of J_2 potential. Effects on the relative position of the satellite due to time-averaged J_2 with corrections model was shown to advocate its implementation for the proposed optimal propellant rendezvous problem. The minimum-propellant-control problem was formulated and addressed using the direct collocation pseudospectral methods. Differential J_2 without corrections model was all analyzed to show the significant errors in the relative position due to the orbital period mismatch and nodal drifts. The desired optimal trajectory of the chaser spacecraft with respect to the tumbling resident space object is sought such that the desired final state matches its position and velocity under its defined tolerances. The effect of J_2 potential is examined on the optimality condition for a defined rendezvous scenario.

Further study is required and will incorporate the the full 6dof model of the chaser spacecraft, where both the rotational and transnational dynamics will be considered. Moreover, to make the capture scenario more realistic collision-avoidance condition will be imposed in form of a path constraint. Along with that docking/capture-enabling conditions will also be incorporated by matching the chaser's and target's docking-station position and velocity vectors. Moreover, optimal-time and optimal-energy conditions will also be studies for the rendezvous scenario to truly find the optimal trajectory for target capture. A nominal validation benchmark will be introduced by using GMAT (General Mission Analysis Tool), an open-source pace mission design tool created by NASA Goddard to optimize and propagate the trajectories under the influence of J_2 disturbance. To fully incorporate the environmental perturbations that affects the proximity operations, the authors would like to add aerodynamic drag forces into the relative equations of motion model. Its combined effect along with J_2 geopotential disturbance will be studied. Optimal trajectories will be planned with all the above constraints defined.

Acknowledgments

The work presented above benefited greatly by the help of Dr. Anil Rao, Associate Professor at University of Florida, Gainesville for all his time and input with any concerns and questions related to GPOPS-II.

REFERENCES

[1] Davis, T. M., and Melanson, D., "XSS-10 Micro-Satellite Floght Demonstration Program" Proceedings ogf the 17th Annual AIAA/USU Conference of Small Satellites, Logan, UT, 11-14 Aug. 2003, pp. 99-99.

[2] David, L,. "Military Micro-Sat Explores Space Inspection, Servicing Technologies" Space.com, www.space.com/businesstechnology/050722_Xss-11_test_html, Technology, 22 July 2005

[3] Dornheim, M. A., Orbital Express to Test Full Autonomy for On-Orbit Service, Aviation Week & Space Technology, www.aviationnow.com/avnow/news/channel_awst_story.jsp?id=news aw0605 06p1.xml, 4 June 2006 [retrieved 20 July 2009].

[4] Friend, R. B., Orbital Express Program Summary and Mission Overview, Proceedings of SPIE: The International Society for Optical Engineering, Vol. 6958, 2008, Paper 695803. doi:10.1117/12.783792

[5] G. Boyarko, Spacecraft guidance strategies for proximity maneuvering and close approach with a tumbling object, PhD, 2010.

[6] G. Boyarko, Y. Oleg, and R. Marcello, Real-time 6dof guidance for of spacecraft proximity maneuver- ing and close approach with a tumbling object, in 2010 AIAA/AAS Astrodynamics Specialist Conference, ser. Guidance, Navigation, and Control and Co-located Conferences. American Institute of Aeronautics and Astronautics, 2010.

[7] G. Boyarko, O. Yakimenko, and M. Romano, Optimal rendezvous trajectories of a controlled spacecraft and a tumbling object, Journal of Guidance, Control, and Dynamics, vol. 34, no. 4, pp. 12391252, 2011.

[8] NASA, DART Mission, http://www.nasa.gov/missions/ - science/dart_into_space.html/

[9] Prussing, J. E., and Conway, B. A., Orbital Mechanics, Oxford Univ. Press, New York, 1993, pp. 139169.

[10] Rao, A. V., Benson, D. A., Darby, C. L., Patterson, M.A., Franscolin, C., Sanders, I., and Huntington, G. T. (2008), "GPOPS: A MATLAB Software for Solving Multiple-Phase Optimal Control Problems Using The Gauss Pseudospectral Method" ACM Transsaction on Mathematical Software

[11] Sedwick, R. J., Miller, D. W., and Kong, E. M. C., Mitigation of Differential Perturbations in Clusters of Formation Flying Satellites, AAS/AIAA Space Flight Mechanics Meeting, American Astronautical Society, AAS Paper 99-124, Feb. 1999.

[12] S. Schweighart and R. Sedwick, "High-Fidality Linearized J_2 Model for Satellite Formation Flight.", Journal of Guidance, Control and Dynamics, Vol.25, No.6, Nov-Dec 2002, pp1073-1080

[13] T. Kasai, M. Oda and T. Suzuki, Results of the ETS-7 Mission Rendezvous Docking and Space Robotics Experiment, in 5th Int. Symp. on Artificial Intelligence, Robotics and Auto. in Space, ESTEC/ESA, Nordwijk, The Netherlands, pp.299-306., 1999.

[14] B. Udrea, and M. Nayak, A Cooperative Multi-Satellite Mission for Controlled Active Debris Removal from Low Earth Orbit, in 2015 IEEE Aerospace Conference, 2015.

BIOGRAPHY

Parv Patel *received his B.S. in Aerospace Engineering from Embry-Riddle Aeronautical University, Daytona Beach, FL concentrating in both Astronautics and Propulsion. He further recieved his M.S. in Astronautical Engineering from the University of Southern California, Los Angeles, CA. He is currently persuing a Ph.D. degree in Astronautical Engineering at University of Southern California. Parv has worked as a Simulation Test Engineer at Gulfstream Aerospace Corp. Savannah, GA. His research interest include near-Earth object exploration, modeling gravitational fields, interplanetary space mission design, invariant manifolds and spacecraft controls.*

Dr. Bogdan Udrea *received his Dipl. Eng. in Aeronautical Engineering from the Polytechnic Institute of Bucharest, Romania in 1990 and his Ph.D. in Aeronautics and Astronautics from the University of Washington in 1999. He is the founder and CEO of VisSidus Technologies, Inc., a company that develops technologies for outer space sustainability. Bogdan has a day job as an Associate Professor of Aerospace Engineering at the Embry-Riddle Aeronautical University and has previously worked as a Control and Navigation Systems Engineer at the European Space Agency. His research interests include spacecraft dynamics and control and space mission design with emphasis on proximity operations, formation flying, near-Earth object exploration and on-board autonomy.*

Michael Nayak *received a B.S. and M.S. in Aerospace Engineering from Embry-Riddle Aeronautical University, Daytona Beach, FL. He is currently pursuing a Ph.D. degree in Earth and Planetary Science at the University of California, Santa Cruz. He is also an active duty Air Force officer, the Chief Scientist of the ARAPAIMA Program, and founder of the aerospace consulting firm Red Sky Research, LLC. Mikey has served as Lead Flight Director and Mission Manager for the Air Force Research Laboratory's Tactical Satellite III and has managed operations for the NASA Earth Science pathfinder CloudSat. He is the recipient of a National Defense Science and Engineering Graduate (NDSEG) Fellowship and the 2013 General Samuel C. Phillips award for the Space and Missile System Center's Outstanding Young Engineer/Scientist.*